Large positive and negative lateral shifts near pseudo-Brewster dip on reflection from a chiral metamaterial slab

Y. Y. Huang,[1,3] **W. T. Dong,**[1] **L. Gao,**[1,4] **and C. W. Qiu**[2,5]

[1] *Jiangsu Key Laboratory of Thin Films, Department of Physics, Soochow University, Suzhou 215006, China*
[2] *Department of Electrical and Computer Engineering, National University of Singapore, 4 Engineering Drive 3, Singapore 117576, Singapore*
[3] *School of Science, Nantong University, Nantong 226000, China*
[4] *leigao@suda.edu.cn*
[5] *eleqc@nus.edu.sg*

Abstract: The lateral shifts from a slab of lossy chiral metamaterial are predicted for both perpendicular and parallel components of the reflected field, when the transverse electric (TE)-polarized incident wave is applied. By introducing different chirality parameter, the lateral shifts can be large positive or negative near the pseudo-Brewster angle. It is found that the lateral shifts from the negative chiral slab are affected by the angle of incidence and the chirality parameter. In the presence of inevitable loss of the chiral slab, the enhanced lateral shifts will be decreased, and the pseudo-Brewster angle will disappear correspondingly. For the negative chiral slab with loss which is invisible for the right circularly polarized (RCP) wave, we find that the loss of the chiral slab will lead to the fluctuation of the lateral shift with respect to the thickness of the chiral slab.The validity of the stationary-phase analysis is demonstrated by numerical simulations of a Gaussian-shaped beam.

OCIS codes: (260.0260) Physical optics; (260.2110) Electromagnetic optics; (160.1585) Chiral media; (120.5700) Reflection; (160.3918) Metamaterials; (350.5500) Propagation.

References and links

1. F. Goos and H. Hänchen, "Ein neuer und fundamentaler Versuch zur Totalreflexion," Ann. Phys. **1**, 333–346 (1947).
2. K. Artmann, "Berechnung der Seitenversetzung des totalreflektierten Strahles," Ann. Phys. **2**, 87–102 (1948).
3. R. H. Renard, "Total reflection: a new evaluation of the Goos-Hänchen shift," J. Opt. Soc. Am. **54**, 1190–1196 (1964).
4. B. R. Horowitz and T. Tamir, "Lateral displacement of a light beam at a dielectric interface," J. Opt. Soc. Am. **61**, 586–594 (1971).
5. F. Bretenaker, A. Le Floch, and L. Dutriaux, "Direct measurement of the optical Goos-Hänchen effect in lasers," Phys. Rev. Lett. **68**, 931–933 (1992).
6. O. Emile, T. Galstyan, A. Le Floch, and F. Bretenaker, "Measurement of the nonlinear Goos-Hänchen effect for Gaussian optical beams," Phys. Rev. Lett. **75**, 1511–1513 (1995).
7. B. M. Jost, A. A. R. Al-Rashed, and B. E. A. Saleh, "Observation of the Goos-Hänchen effect in a phase-conjugate mirror," Phys. Rev. Lett. **81**, 2233–2235 (1998).
8. A. Madrazo and M. Nieto-Veperinas, "Detection of subwavelength Goos-Hänchen shifts from near-field intensities: a numerical simulation," Opt. Lett. **20**, 2445–2447 (1995).
9. L. G. Wang, H. Chen, N. H. Liu, and S. Y. Zhu, "Negative and positive lateral shift of a light beam reflected from a grounded slab," Opt. Lett. **31**, 1124–1126 (2006).

#139089 - $15.00 USD Received 2 Dec 2010; revised 7 Jan 2011; accepted 10 Jan 2011; published 11 Jan 2011

10. C. F. Li, “Negative lateral shift of a light beam transmitted through a dielectric slab and interaction of boundary effects,” Phys. Rev. Lett. **91**, 133903–133906 (2003).
11. M. Merano, A. Aiello, C. W. Hooft, M. P. van Exter, E. R. Eliel, and J. P. Woerdman, “Observation of Goos-Hänchen shifts in metallic reflection,” Opt. Express **15**, 15928–15934 (2007).
12. D. J. Hoppe and Y. Rahmat-Samii, “Gaussian beam reflection at a dielectric-chiral interface,” J. Electromagn. Waves Appl. **6**, 603–624 (1992).
13. R. A. Depine and N. E. Bonomo, “Goos-Hänchen lateral shift for Gaussian beams reflected at achiral-chiral interfaces,” Optik **103**, 37–41 (1996).
14. F. Wang and A. Lakhtakia, “Lateral shifts of optical beams on reflection by slanted chiral sculptured thin films,” Opt. Commun. **235**, 107–132 (2004).
15. W. T. Dong, L. Gao, and C. W. Qiu, “Goos-Hänchen shift at the surface of chiral negative refractive media,” Prog. Electromagn. Res., PIER **104**, 255–263 (2009).
16. W. J. Wild and C. L. Giles, “Goos-Hänchen shifts from absorbing media,” Phys. Rev. A **25**, 2099–2101 (1982).
17. E. Pfleghaar, A. Marseille, and A. Weis, “Quantitative investigation of the effect of resonant absorbers on the Goos-Hänchen Shift,” Phys. Rev. Lett. **70**, 2281–2284 (1993).
18. B. Zhao and L. Gao, “Temperature-dependent Goos-Hänchen shift on the interface of metal/dielectric composites,” Opt. Express **17**, 21433–21441 (2009).
19. F. Lima, T. Dumelow, J. A. P. Costa, and E. L. Albuquerque, “Lateral shift of far infrared radiation on normal incidence reflection off an antiferromagnet,” Europhys. Lett. **83**, 17003 (2008).
20. P. R. Berman, “Goos-Hänchen shift in negatively refractive media,” Phys. Rev. E **66**, 067603 (2002).
21. J. A. Kong, B. K. Wu, and Y. Zhang, “Lateral displacement of a Gaussian beam reflected from a grounded slab with negative permittivity and permeability,” Appl. Phys. Lett. **80**, 2084–2086 (2002).
22. A. Lakhtakia, “On planewave remittances and Goos-Hänchen shifts of planar slabs with negative real permittivity and permeability”, Electromagnetics **23**, 71-75 (2003).
23. D. R. Pendry, “A chiral route to negative refraction,” Science **306**, 1353–1355 (2004).
24. C. W. Qiu, N. Burokur, S. Zouhdi, and L. W. Li, “Chiral nihility effects on energy flow in chiral materials,” J. Opt. Soc. Am. A **25**, 53–63 (2008).
25. C. W. Qiu, H. Y. Yao, L. W. Li, S. Zouhdi, and S. T.Yeo, “Backward waves in magnetoelectrically chiral media: propagation, impedance and negative refraction,” Phys. Rev. B **75**, 155120 (2007).
26. S. Zhang, Y. S. Park, J. S. Li, X. C. Lu, W. L. Zhang, and X. Zhang, “Negative refractive index in chiral metamaterials,” Phys. Rev. Lett. **102**, 023901 (2009).
27. J. F. Zhou, J. F. Dong, N. B. Wang, T. Koschny, M. Kafesaki, and C. M. Soukoulis, “Negative refractive index due to chirality,” Phys. Rev. B **79**, 121104 (2009).
28. I. V. Lindell, A. H. Sihvola, S. A. Tretyakov, and A. J. Viitanen, *Electromagnetic Waves in Chiral and Bi-isotropic Media* (Artech House, Boston) (1994).
29. J. F. Dong and B. Liu, “Goos-Hänchen shift at the surface of the chiral negative refraction medium,” Proceedings of the 2008 International workshop on metamaterials, Nanjing, China, 98–101 (2008).
30. S. Bassiri, C. H. Papas, and N. Engheta, “Electromagnetic wave propagation through a dielectric-chiral interface and through a chiral slab,” J. Opt. Soc. Am. A **5**, 1450–1459 (1988).
31. S. Bassiri, C. H. Papas, and N. Engheta, “Electromagnetic wave propagation through a dielectric-chiral interface and through a chiral slab: errata,” J. Opt. Soc. Am. A **7**, 2154–2155 (1990).
32. M. McGuirk and C. K. Carniglia, “An angular spectrum representation approach to the Goos-Hänchen shift,” J. Opt. Soc. Am **67**, 103–107 (1977).
33. M. Cheng, R. Chen, and S. Feng, “Lateral shifts of an optical beam in an anisotropic metamaterial slab,” Eur. Phys. J. D **50**, 81–85 (2008).
34. H. Huang, Y. Fan, B. I. Wu, and J. A. Kong, “Positively and negatively large Goos-Hänchen lateral displacement from a symmetric gyrotropic slab,” Appl. Phys. A **94**, 917–922 (2009).
35. Y. Tamayama, T. Nakanishi, K. Sugiyama, and M.Kitano, “An invisible medium for circularly polarized electromagnetic waves,” Opt. Express **16**, 20869–20875 (2008).
36. C. F. Li and Q. Wang, “Prediction of simultaneously large and opposite generalized Goos-Hänchen shifts for TE and TM light beams in an asymmetric double-prism configuration,” Phys. Rev. E **69**, 055601 (2004).
37. Y. Jin and S. L. He, “Focusing by a slab of chiral medium,” Opt. Express **13**, 4974–4979 (2005).
38. Q. Cheng and T. J. Cui, “Negative refractions in uniaxially anisotropic chiral media,” Phys. Rev. B **73**, 113104 (2006).
39. T. G. Mackay and A. Lakhtakia, “Negative refraction, negative phase velocity, and counterposition in bianisotropic meterials and metamaterials,” Phys. Rev. B **79**, 235121 (2009).
40. C. W. Qiu, H. Y. Yao, L. W. Li, T. S. Yeo, and S. Zouhdi, “Routes to left-handed media by magnetoelectric couplings,” Phys. Rev. B **75**, 245214 (2007).
41. H. M. Lai and S. W. Chan, “Large and negative Goos-Hänchen shift near the Brewster dip on reflection from weakly absorbing media,” Opt. Lett. **27**, 680–682 (2002).
42. K. Yu. Bliokh and Yu. P. Bliokh, “Polarization, transverse shifts, and angular momentum conservation laws in partical reflection and refraction of an electromagnetic wave packet, ” Phys. Rev. E **75**, 066609 (2007).

#139089 - $15.00 USD Received 2 Dec 2010; revised 7 Jan 2011; accepted 10 Jan 2011; published 11 Jan 2011

43. C. F. Li, "Unified theory for Goos-Hänchen and Imbert-Fedorov effects," Phys. Rev. A **76**, 013811 (2007).
44. A. Aiello and J. P. Woerdman, "Role of beam propagation in Goos-Hänchen and Imbert-Fedorov shifts," Opt. Lett. **33**, 1437–1439 (2008),

1. Introduction

The Goos-Hänchen (GH) effect [1] has been analyzed both theoretically [2–4] and experimentally [5–7]. This phenomenon has already been extended to other areas such as acoustics, surface optics, nonlinear optics, and quantum mechanics. Furthermore, with the development of near-field scanning optical microscopy and lithography [8], the GH shift has attracted more and more attention for potential device applications in optical modulations. On the other hand, there exist some other lateral shifts, which are quite different from the GH effect, since the magnitude of the reflection coefficient is dependent on the angle of incidence for the partial reflection. For instance, at an oblique incidence, the lateral shifts were found to be large positive or negative for both reflected and transmitted beams in different media such as dielectric surfaces or slabs [9, 10], metal surfaces [11], dielectric-chiral surface [12–15], absorptive media [16–18], and so on. Later, Lima *et al* reported that a normally incident beam reflected from an antiferromagnet can result in a lateral shift too [19].

Recently, the lateral shift associated with metamaterial [20–22] is of interest owing to its very unusual properties. For these metamaterials, their permittivity and permeability are both negative. On the other hand, Pendry found that the chiral medium with the Swiss roll structure may also possess negative refraction [23]. After that, chiral metamaterial with negative refraction (or negative chiral metatamaterial) received great interest from both theoretical [24, 25] and experimental views [26, 27]. Since the realistic chiral material is dissipative, in this paper, we would like to investigate the lateral shift of the reflected beam from a chiral metamaterial slab with inherent loss. We demonstrate that these perpendicular and parallel polarized waves can, to the first order, be independently separated, each with its own lateral shifts. As a consequence, the validity of the stationary phase method is proved and further confirmed with the numerical simulation. We predict that the lateral shift near the angle of the pseudo-Brewster dip from such a slab can be large, and both positive and negative lateral shifts are possible. It is also shown that the lateral shift depends on the thickness of the slab, the angle of the incident wave and the constitutive parameters of the negative chiral metemeterials. Throughout the paper, only transverse-electric (TE) polarized incident wave is discussed below, and the results for transverse-magnetic (TM) polarized wave can be easily obtained in the same way.

2. Formulation

2.1. Reflection and transmission amplitudes

The configuration for the chiral slab is shown in Fig. 1. We assume that a linearly TE polarized wave is incident at an angle θ_i upon the surface of a chiral slab with the thickness d. For simplicity, time dependence $\exp(-i\omega t)$ is applied and suppressed. The constitutive relations of the chiral slab are defined as [28]

$$\mathbf{D} = \varepsilon\varepsilon_0\mathbf{E} + i\kappa\sqrt{\varepsilon_0\mu_0}\mathbf{H}, \quad \mathbf{B} = \mu\mu_0\mathbf{H} - i\kappa\sqrt{\varepsilon_0\mu_0}\mathbf{E}, \tag{1}$$

where κ is the chirality parameter, ε and μ are the relative permittivity and permeability of the chiral medium, respectively (ε_0 and μ_0 are the permittivity and permeability in vacuum). The electric and magnetic fields of an incident TE wave can be written as

$$\mathbf{E_i} = E_i\mathbf{e_y} = E_0\mathbf{e_y}\exp[ik_i(\cos\theta_i z + \sin\theta_i x)], \quad \mathbf{H_i} = \sqrt{\frac{\varepsilon_0}{\mu_0}}E_i(-\cos\theta_i\mathbf{e_x} + \sin\theta_i\mathbf{e_z}), \tag{2}$$

Received 2 Dec 2010; revised 7 Jan 2011; accepted 10 Jan 2011; published 11 Jan 2011

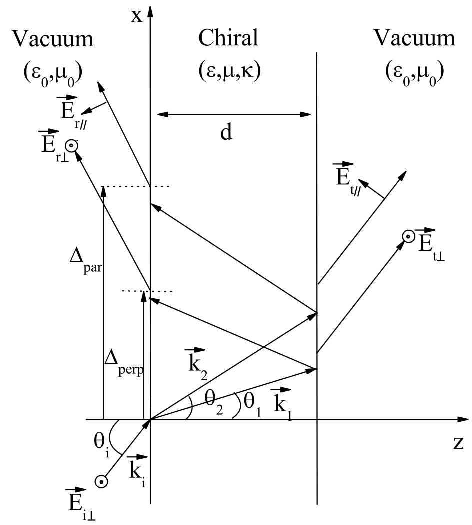

Fig. 1. Schematic diagram of a light beam propagating through the chiral slab placed in free space.

with the wave number $k_i = k_0 \equiv \omega/c$. It is known that, an electric or magnetic excitation will produce both the electric and magnetic polarizations in a chiral material simultaneously. As a consequence, the reflected wave must be a combination of both perpendicular and parallel components in order to satisfy the boundary conditions. In our paper, the linearly polarized incident wave is considered, and then we express the reflected wave in terms of the combination of the perpendicular and parallel polarized waves [12, 13, 29]. Then, the electric and magnetic fields of the reflected wave are expressed as,

$$\mathbf{E_r} = E_0[R_\perp \mathbf{e_y} + R_\parallel(-\cos\theta_i \mathbf{e_x} - \sin\theta_i \mathbf{e_z})]\exp[ik_i(-\cos\theta_i z + \sin\theta_i x)], \tag{3}$$

$$\mathbf{H_r} = \sqrt{\frac{\varepsilon_0}{\mu_0}} E_0[R_\parallel \mathbf{e_y} + R_\perp(\cos\theta_i \mathbf{e_x} + \sin\theta_i \mathbf{e_z})]\exp[ik_i(-\cos\theta_i z + \sin\theta_i x)], \tag{4}$$

where $R_\perp$ and $R_\parallel$ are, respectively, the reflected coefficients associated with perpendicular and parallel components. Here we note that for linearly polarized incident wave, when the angle of incidence is the Brewster angle, the reflected wave is still linearly polarized but its plane of polarization is rotated with respect to the plane of polarization of the incident wave [28, 30, 31], which explains the phase difference between perpendicular and parallel components.

On the other hand, there are two propagation modes inside the slab: a right circularly polarized (RCP) wave with the phase velocity ω/k_1 and a left circularly polarized (LCP) wave with the phase velocity ω/k_2. The wave numbers k_1 and k_2 have the form $k_{1,2} = k_0(\sqrt{\varepsilon}\sqrt{\mu} \pm \kappa)$ and the refractive indices of the two eigen-waves are $n_{1,2} = \sqrt{\varepsilon}\sqrt{\mu} \pm \kappa$ [28]. It is evident that for $\kappa > \sqrt{\varepsilon}\sqrt{\mu}$, which can occur at least at or near the resonant frequency of the permittivity of a chiral medium [24], the refraction index $n_1 \equiv \sqrt{\varepsilon}\sqrt{\mu} + \kappa$ will still be positive, but the refraction index $n_2 \equiv \sqrt{\varepsilon}\sqrt{\mu} - \kappa$ will become negative. Correspondingly, negative refraction will arise for LCP wave. In the chiral slab, there exist four waves in total: two propagating toward the interface $z = d$ and the other two propagating toward the interface $z = 0$ (see Fig. 1). The electric and magnetic fields of these waves propagating inside the chiral medium toward the interface $z = d$ are written as,

$$\mathbf{E_c^+} = \mathbf{E_{cr}^+} + \mathbf{E_{cl}^+} \quad \text{and} \quad \mathbf{H_c^+} = i\eta^{-1}\left(\mathbf{E_{cl}^+} - \mathbf{E_{cr}^+}\right), \tag{5}$$

with $\mathbf{E_{cr}^+} = E_0[A_1 i\mathbf{e_y} + A_1(\cos\theta_1\mathbf{e_x} - \sin\theta_1\mathbf{e_z})]\exp[ik_1(\cos\theta_1 z + \sin\theta_1 x)]$, $\mathbf{E_{cl}^+} = E_0[-A_2 i\mathbf{e_y} + A_2(\cos\theta_2\mathbf{e_x} - \sin\theta_2\mathbf{e_z})]\exp[ik_2(\cos\theta_2 z + \sin\theta_2 x)]$, and $\eta = \sqrt{\mu/\varepsilon}$.

Similarly, the total electromagnetic fields of the other two waves toward the interface $z = 0$ are

$$\mathbf{E_c^-} = \mathbf{E_{cr}^-} + \mathbf{E_{cl}^-} \quad \text{and} \quad \mathbf{H_c^-} = i\eta^{-1}\left(\mathbf{E_{cl}^-} - \mathbf{E_{cr}^-}\right), \tag{6}$$

with $\mathbf{E_{cr}^-} = E_0[B_1 i\mathbf{e_y} + B_1(-\cos\theta_1\mathbf{e_x} - \sin\theta_1\mathbf{e_z})]\exp[ik_1(-\cos\theta_1 z + \sin\theta_1 x)]$, and $\mathbf{E_{cl}^-} = E_0[-B_2 i\mathbf{e_y} + B_2(-\cos\theta_2\mathbf{e_x} - \sin\theta_2\mathbf{e_z})]\exp[ik_2(-\cos\theta_2 z + \sin\theta_2 x)]$. In addition, in Eqs. (5) and (6), $A_{1(2)}$ and $B_{1(2)}$ are the transmitted coefficients, and $\theta_{1(2)}$ denote the refracted angles of the two eigen-waves in the chiral slab, respectively.

Outside the slab ($z > d$), the total transmitted wave can be expressed as

$$\mathbf{E_t} = E_0[T_\perp\mathbf{e_y} + T_\parallel(\cos\theta_t\mathbf{e_x} - \sin\theta_t\mathbf{e_z})]\exp[ik_i(\cos\theta_t z + \sin\theta_t x)], \tag{7}$$

$$\mathbf{H_t} = \sqrt{\frac{\varepsilon_0}{\mu_0}}E_0[T_\parallel\mathbf{e_y} + T_\perp(-\cos\theta_t\mathbf{e_x} + \sin\theta_t\mathbf{e_z})]\exp[ik_i(\cos\theta_t z + \sin\theta_t x)], \tag{8}$$

where θ_t is the transmitted angle, $T_\perp$ and $T_\parallel$ are coefficients associated with perpendicular and parallel components of the transmitted wave.

The coefficients $R_\perp$, $R_\parallel$, $T_\perp$, and $T_\parallel$ are determined by matching the boundary conditions at two interfaces $z = 0$ and $z = d$, and the following matrix can be obtained,

$$\begin{pmatrix} [\Psi]_{11} & [\Psi]_{12} \\ [\Psi]_{21} & [\Psi]_{22} \end{pmatrix} \bullet \begin{pmatrix} R_\perp \\ R_\parallel \\ T_\perp \\ T_\parallel \end{pmatrix} = \begin{pmatrix} i\eta\cos\theta_i + i\cos\theta_1 \\ -i\eta\cos\theta_i + i\cos\theta_1 \\ -i\eta\cos\theta_i - i\cos\theta_2 \\ i\eta\cos\theta_i - i\cos\theta_2 \end{pmatrix}, \tag{9}$$

where

$$[\Psi]_{11} = \begin{pmatrix} i(\eta\cos\theta_i - \cos\theta_1) & -\cos\theta_i + \eta\cos\theta_1 \\ -i(\eta\cos\theta_i + \cos\theta_1) & \cos\theta_i + \eta\cos\theta_1 \end{pmatrix} \tag{10}$$

$$[\Psi]_{21} = \begin{pmatrix} i(-\eta\cos\theta_i + \cos\theta_2) & -\cos\theta_i + \eta\cos\theta_2 \\ i(\eta\cos\theta_i + \cos\theta_2) & \cos\theta_i + \eta\cos\theta_2 \end{pmatrix} \tag{11}$$

$$[\Psi]_{12} = \begin{pmatrix} i(\eta\cos\theta_i + \cos\theta_1)e^{i(k_{iz}-k_{1z})d} & (-\cos\theta_i - \eta\cos\theta_1)e^{i(k_{iz}-k_{1z})d} \\ i(-\eta\cos\theta_i + \cos\theta_1)e^{i(k_{iz}+k_{1z})d} & (\cos\theta_i - \eta\cos\theta_1)e^{i(k_{iz}+k_{1z})d} \end{pmatrix} \tag{12}$$

$$[\Psi]_{22} = \begin{pmatrix} -i(\eta\cos\theta_i + \cos\theta_2)e^{i(k_{iz}-k_{2z})d} & (-\cos\theta_i - \eta\cos\theta_2)e^{i(k_{iz}-k_{2z})d} \\ i(\eta\cos\theta_i - \cos\theta_2)e^{-i(k_{iz}+k_{2z})d} & (\cos\theta_i - \eta\cos\theta_2)e^{i(k_{iz}+k_{2z})d} \end{pmatrix}. \tag{13}$$

The analytic solutions to four coefficients can be obtained after some lengthy mathematic manipulations, but the final results are too complicated to be reproduced here.

2.2. *Stationary phase method for chiral slab*

Next, in order to derive the approximate expressions for the lateral shift from the chiral slab, we adopted the angular spectrum representation approach [32]. We consider the two-dimensional (2D) incident TE wave as a sum of plane waves,

$$\mathbf{E_i}(x, z = 0) = \mathbf{e_y}\int_{-\infty}^{\infty} A(k_x)\exp(ik_x x)\mathrm{d}k_x, \tag{14}$$

#139089 - $15.00 USD Received 2 Dec 2010; revised 7 Jan 2011; accepted 10 Jan 2011; published 11 Jan 2011

where $A(k_x)$ is the amplitude angular-spectrum distribution. Then, the reflected field admits the form,

$$\begin{aligned}\mathbf{E_r}(x,z=0) &= \mathbf{e_y}\int_{-\infty}^{\infty} R_\perp(k_x)A(k_x)\exp(ik_xx)\mathrm{d}k_x \\ &\quad -\int_{-\infty}^{\infty}\left[\mathbf{e_x}\sqrt{1-\left(\frac{k_x}{k_0}\right)^2}+\mathbf{e_z}\frac{k_x}{k_0}\right]R_\parallel(k_x)A(k_x)\exp(ik_xx)\mathrm{d}k_x. \qquad (15)\end{aligned}$$

For simplicity, let $R_j(k_x) = \rho_j(k_x)\exp[i\Phi_j(k_x)]$ ($j = \perp, \parallel$), where $\rho_j(k_x)$ is the reflection amplitude and $\Phi_j(k_x)$ is the phase of the reflectance.

Note that if the incident light beam is well collimated and wide enough, $A(k_x)$ should be sharply peaked around k_{x0}. In the case of a wide enough beam, there will only be significant contributions to the integrals of Eq. (15) within a narrow distribution of k_x values around k_{x0}. As a consequence, we can expand $\rho_j(k_x)$, $\Phi_j(k_x)$, and the quantity for the polarization direction $\mathbf{e_x}\sqrt{1-(k_x/k_0)^2}+\mathbf{e_z}k_x/k_0$ as a Taylor series [19]. Keeping terms to the first order of $\Delta k_x = k_x - k_{x0}$, we have

$$\rho_j(k_x) \approx \rho_j(k_{x0}) + \Delta k_x \rho_j'(k_{x0}), \qquad \Phi_j(k_x) \approx \Phi_j(k_{x0}) + \Delta k_x \Phi_j'(k_{x0}), \qquad (16)$$

and,

$$\begin{aligned}\mathbf{e_x}\sqrt{1-\left(\frac{k_x}{k_0}\right)^2}+\mathbf{e_z}\frac{k_x}{k_0} &\approx \left(\mathbf{e_x}\sqrt{1-\left(\frac{k_{x0}}{k_0}\right)^2}+\mathbf{e_z}\frac{k_{x0}}{k_0}\right)+\Delta k_x\left(\mathbf{e_x}\frac{-1}{\sqrt{k_0^2-k_{x0}^2}}\frac{k_{x0}}{k_0}+\mathbf{e_z}\frac{1}{k_0}\right) \\ &\equiv \mathbf{e}_\parallel + \Delta k_x \mathbf{e}_{\parallel\mathbf{2}}. \qquad (17)\end{aligned}$$

Substituting Eq. (17) into Eq. (15), we have the perpendicular component (along $y-$axis) and parallel component (in $x-z$ plane) for the electric field of the reflected beam, which can be rewritten as

$$\mathbf{E_r}(x,z=0) = \mathbf{e_y}E_\perp^r - [\mathbf{e}_\parallel E_\parallel^r + \mathbf{e}_{\parallel\mathbf{2}}E_{\parallel 2}^r], \qquad (18)$$

with

$$E_{\perp(\parallel)}^r(x,z=0) = \int_{-\infty}^{\infty} R_{\perp(\parallel)}(k_x)A(k_x)\exp(ik_xx)\mathrm{d}k_x, \qquad (19)$$

$$E_{\parallel 2}^r(x,z=0) = \int_{-\infty}^{\infty} \Delta k_x R_\parallel(k_x)A(k_x)\exp(ik_xx)\mathrm{d}k_x. \qquad (20)$$

Substitution of Eq. (16) into Eqs. (19) and (20) gives

$$\begin{aligned}E_{\perp(\parallel)}^r(x,z=0) &= r_{\perp(\parallel)}(k_{x0})\int_{-\infty}^{\infty} A(k_x)\exp\{ik_x[x+\Phi_{\perp(\parallel)}'(k_{x0})]\}\mathrm{d}k_x \\ &\quad + r_{\perp(\parallel)}'(k_{x0})\int_{-\infty}^{\infty}(k_x-k_{x0})A(k_x)\exp\{ik_x[x+\Phi_{\perp(\parallel)}'(k_{x0})]\}\mathrm{d}k_x, \quad (21)\end{aligned}$$

$$\begin{aligned}E_{\parallel 2}^r(x,z=0) &= r_\parallel(k_{x0})\int_{-\infty}^{\infty}(k_x-k_{x0})A(k_x)\exp\{ik_x[x+\Phi_\parallel'(k_{x0})]\}\mathrm{d}k_x \\ &\quad + r_\parallel'(k_{x0})\int_{-\infty}^{\infty}(k_x-k_{x0})^2A(k_x)\exp\{ik_x[x+\Phi_\parallel'(k_{x0})]\}\mathrm{d}k_x, \qquad (22)\end{aligned}$$

with $r_j(k_{x0}) = \rho_j(k_{x0})\exp[i\Phi_j(k_{x0}) - ik_{x0}\Phi_j'(k_{x0})]$ and $r_j'(k_{x0}) = \rho_j'(k_{x0})\exp[i\Phi_j(k_{x0}) - ik_{x0}\Phi_j'(k_{x0})]$.

#139089 - $15.00 USD Received 2 Dec 2010; revised 7 Jan 2011; accepted 10 Jan 2011; published 11 Jan 2011

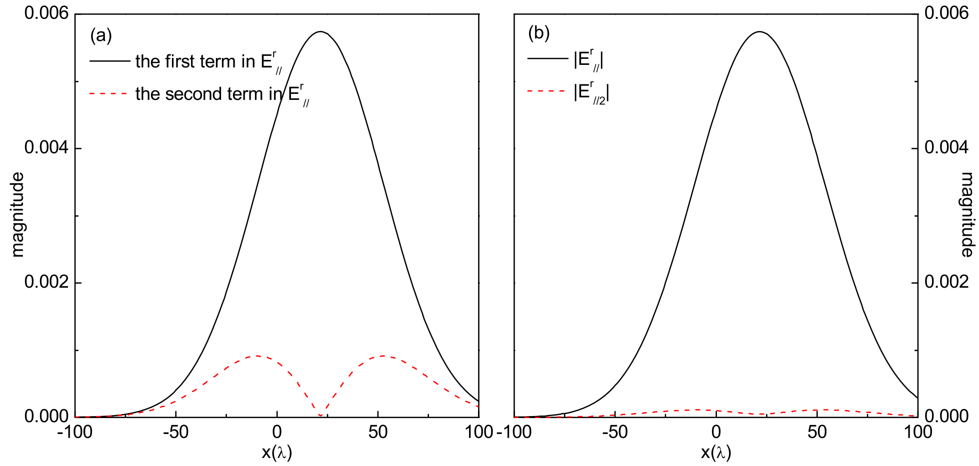

Fig. 2. the magnitude of (a) the first and second components in $E^r_\parallel$ (see Eq. (21)) and (b) $E^r_\parallel$ in Eq. (21) and $E^r_{\parallel 2}$ in Eq. (22) as a function of x. The relevant parameters are $\varepsilon = 0.64+0.01i$, $\mu = 1+0.02i$, $\kappa = 2$, $w_0 = 20\lambda$, $d = 1.5\lambda$, and $\theta_i = 50^o$.

For a Gaussian-shaped incident beam, the electric field of the incident beam has the form $E_i(x,z=0) = \exp(-x^2/2w_x^2 + ik_{x0}x)$, where $w_x = w_0 \sec\theta_i$, w_0 is the beam width at the waist. As a consequence, from Eq. (14), the amplitude angular-spectrum distribution is derived to be $A(k_x) = w_x/(2\pi)^{1/2}\exp[-w_x^2(k_x-k_{x0})^2/2]$ [10, 12]. Since we have assumed that the beam is well collimated and wide enough, $A(k_x)$ should be a sharply distributed Gaussian function around k_{x0}. By comparing these two terms on the right hand of Eq. (21), it is expected that the first term dominates for a narrow distribution of k_x values, and we can ignore the second term as a first approximation. In Fig. 2(a), it is numerically demonstrated that the second term can be regarded as a perturbation to the first term. Similarly, comparing the magnitude of $E^r_{\parallel 2}$ [see Eq. (20) or Eq. (22)] with that of $E^r_\parallel$ [see Eq. (19) or Eq. (21)], one can ignore $E^r_{\parallel 2}$, as shown in Fig. 2(b). Therefore, as a first approximation, we have,

$$\begin{aligned}\mathbf{E_r}(x,z=0) \quad &= \quad \mathbf{e_y}E^r_\perp - \mathbf{e}_\parallel E^r_\parallel = \mathbf{e_y} r_\perp(k_{x0})\int_{-\infty}^{\infty} A(k_x)\exp\{ik_x[x+\Phi'_\perp(k_{x0})]\}\mathrm{d}k_x \\ &\quad -\mathbf{e}_\parallel r_\parallel(k_{x0})\int_{-\infty}^{\infty} A(k_x)\exp\{ik_x[x+\Phi'_\parallel(k_{x0})]\}\mathrm{d}k_x. \end{aligned} \tag{23}$$

Note that the integral for the reflected beam $E^r_{\perp(\parallel)}$ is identical to that for the incident beam [Eq. (14)], except that x is replaced by $x+\Phi'_{\perp(\parallel)}(k_{x0})$. This indicates that the center of the peak of the reflected field is given by

$$x+\Phi'_{\perp(\parallel)}(k_{x0}) = 0, \tag{24}$$

and correspondingly, the reflected beam is shifted along the surface of the chiral slab by a distance $\Delta_{\perp(\parallel)}$,

$$\Delta_{\perp(\parallel)} = -\left.\frac{\mathrm{d}\Phi_{\perp(\parallel)}(k_x)}{\mathrm{d}k_x}\right|_{k_{x0}}. \tag{25}$$

Here we mention that for chiral materials, the reflected wave will have two polarizations (perpendicular and parallel components) due to the chirality. Fortunately, these two polarized

#139089 - $15.00 USD Received 2 Dec 2010; revised 7 Jan 2011; accepted 10 Jan 2011; published 11 Jan 2011

reflected waves can be independently separated, each with its own magnitude and lateral shift. Note that the derivation is for the chiral materials, but it is actually equivalent to the classic expression of stationary phase method [2]. Actually, although Artmann's formula was derived initially for an isotropic material, it was further successfully used to investigate lateral shifts in antiferromagnet with anisotropic dielectric tensors [19], an anisotropic metamaterial slab [33], and a gyrotropic slab [34].

3. Results and discussion

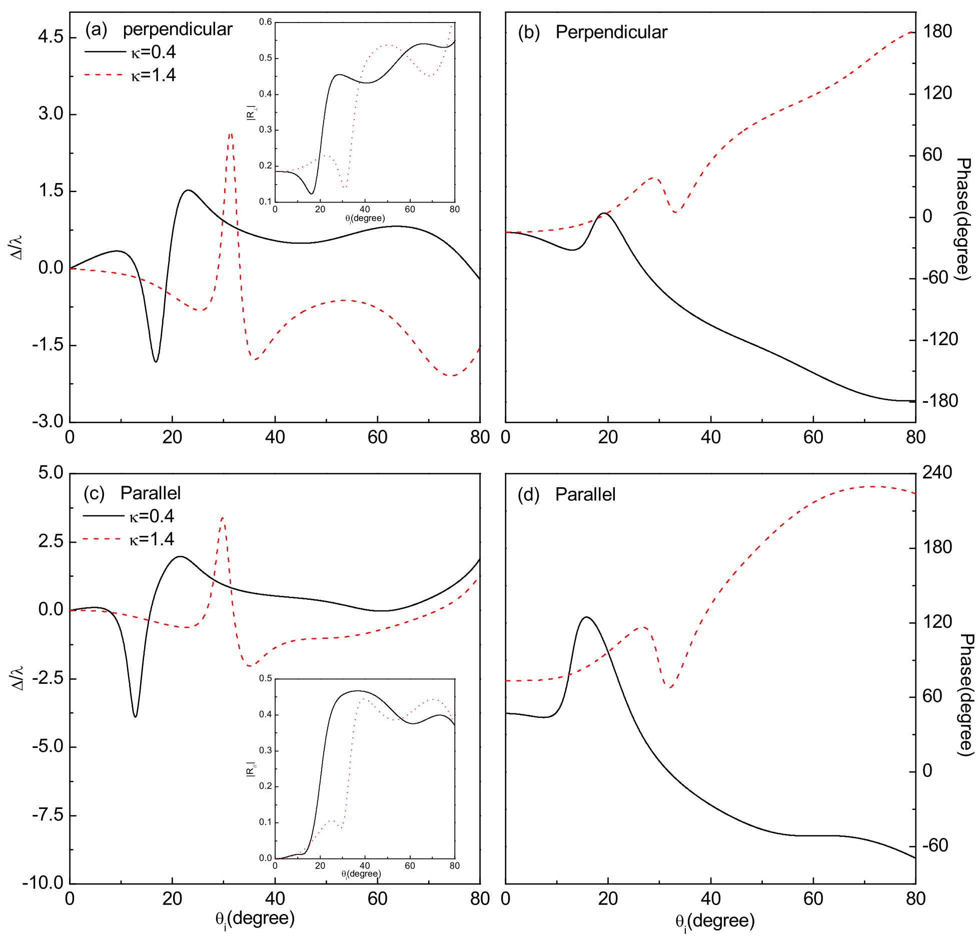

Fig. 3. The dependences of the lateral shifts Δ/λ (a,c) and the phases of the reflection coefficients (b,d) for perpendicular (a,b) and parallel components (c,d) on the angle of incidence θ_i. The insets of (a) and (c) show the absolute values of perpendicular and parallel reflection coefficients, respectively. Solid line and dashed line correspond to positive chiral slab with $\kappa = 0.4$ and negative chiral slab with $\kappa = 1.4$.

We are now able to present numerical results on the lateral shifts of the chiral slab. Actual chiral materials are usually dissipative in the resonant frequency in which the chirality is significant but has a lossy part. In this connection, the parameters are taken to be $\varepsilon = 0.64 + 0.01i$, $\mu = 1 + 0.02i$, $\omega = 2\pi \times 10$ GHz, and $d = 1.5\lambda$ [12]. Without loss of generality, we consider two types of chiral slabs: (1) a positive (conventional) chiral slab with $\kappa = 0.4$, whose refraction

#139089 - $15.00 USD Received 2 Dec 2010; revised 7 Jan 2011; accepted 10 Jan 2011; published 11 Jan 2011

indices of RCP and LCP waves are both positive ($\mathrm{Re}(n_1) = 1.2$ and $\mathrm{Re}(n_2) = 0.4$); (2) a negative chiral slab with $\kappa = 1.4$ whose refraction indices of RCP wave and LCP wave are $\mathrm{Re}(n_1) = 2.2$ and $\mathrm{Re}(n_2) = -0.6$, respectively. For the two cases above, there are no critical angles for RCP waves, but for LCP waves, there exists the critical angle at $\theta_c \simeq 23.6^\circ$ for a positive chiral slab and $\theta_c \simeq 37^\circ$ for a negative chiral slab. Under such critical situations, only LCP waves in the chiral slab become evanescent waves when the angle of incidence exceeds the critical angle, while the RCP waves will still propagate through the chiral slab. Correspondingly, the angle of incidence is defined as pseudo-critical angle. However, the true total internal reflection will never arise under these parameters.

Figure 3(a) and 3(c) show the lateral shifts of the reflected waves for both perpendicular and parallel components. In addition, the insets show, respectively, the absolute values of perpendicular and parallel reflection coefficients for two cases. It is easily found that there is a dip in each reflection curve, at which $|R|$ reaches the minimum. The corresponding angle of incidence is defined as the pseudo-Brewster angle. Note that the pseudo-Brewster angles for both perpendicular and parallel components are always smaller than the pseudo-critical angles. From Fig. 3(a) and 3(c), we clearly see that the behavior of the lateral shifts for perpendicular and parallel components are similar, and the shifts will be greatly enhanced near the angle of pseudo-Brewster dip. To one's interest, there exist large negative (positive) lateral shifts near the angle of pseudo-Brewster dip for the positive (negative) chiral slab. The phenomenon can be easily explained in terms of the change of phases, as shown in Fig. 3(b) and 3(d). Near the angle of pseudo-Brewster dip, the phase of reflection experiences a distinct sharp variation, which decreases quickly for the negative chiral slab. As a result, one predicts a large positive lateral shift for a negative chiral slab. On the other hand, for the positive chiral slab, both components have negative lateral shifts near the angle of pseudo-Brewster dip, and then experience small positive shifts over other angles of incidence. We conclude that the lateral shifts of both perpendicular and parallel components can be greatly enhanced near the pseudo-Brewster angle for both the positive and negative chiral slabs, and the dependence of lateral shifts on the angle of incidence θ_i for a negative chiral slab is opposite to that for a positive chiral slab.

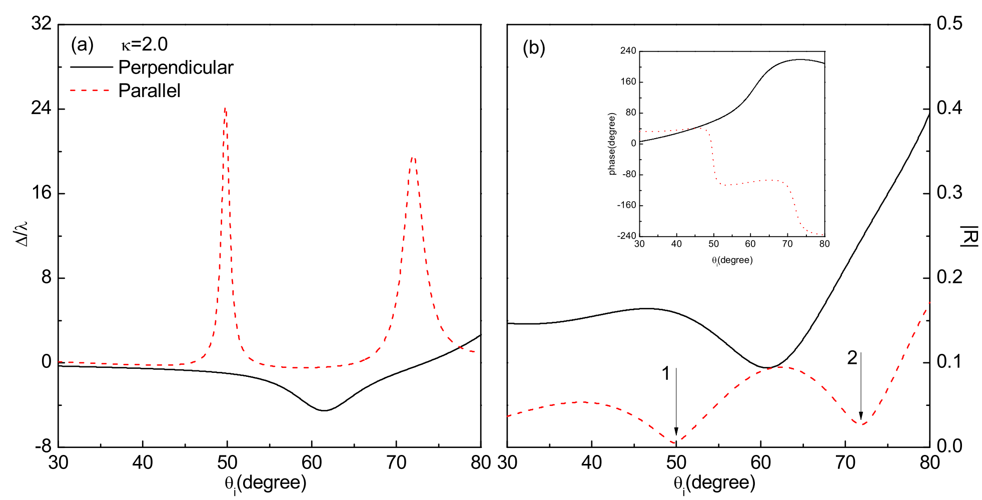

Fig. 4. (a) Δ/λ and the absolute values of reflection coefficients as a function of θ_i for a typical negative chiral slab. The inset of (b) is the phase of reflection coefficients.

Lateral shifts and the reflection amplitudes of reflected waves for perpendicular and parallel components from a negative chiral slab with a large chirality parameter $\kappa = 2.0$ are shown in

#139089 - $15.00 USD Received 2 Dec 2010; revised 7 Jan 2011; accepted 10 Jan 2011; published 11 Jan 2011

Fig. 4. In this situation, there are no critical angles for both the RCP and LCP waves. It can be seen that there is only one dip in the perpendicular reflection curve, at which the reflection coefficient reaches a minimal magnitude and the corresponding phase is monotonically increasing as a function of the angle of incidence [see Fig. 4(b)]. As a consequence, one expects that the lateral shift of the reflected perpendicular component has a negative peak near the angle of the dip [see Fig. 4(a)]. In contrast, there are two dips for the parallel component, where the absolute values of the reflection coefficient are very close to zero, and the corresponding phase in the vicinity of these two dips monotonically decreases quickly [see the inset in Fig. 4(b)]. Thus the shifts of the parallel component can be greatly enhanced to be large positive near the pseudo-Brewster angles where the phase decreases. Note that the lateral shift can be one order in magnitude greater than the wavelength. By comparing Fig. 3 to Fig. 4, we find that for the negative chiral slab, as the chirality parameter becomes large, the lateral shifts for the perpendicular component can change from positive to negative, while they are always positive for the parallel component. But the number of the peaks of the enhanced lateral shifts may increase at the angles of the dips, due to the resonant conditions.

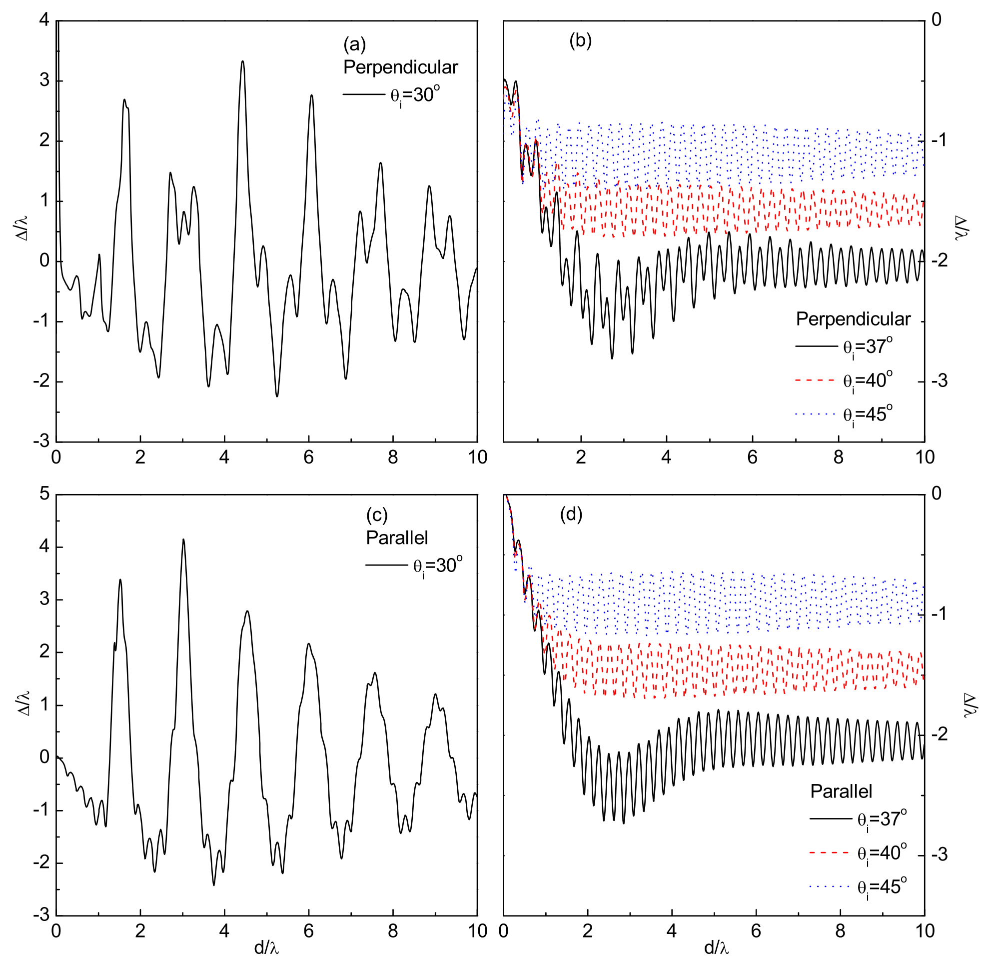

Fig. 5. Δ/λ as a function of d of the negative chiral slab for different θ_i. Reflected perpendicular component for (a) and (b) and reflected parallel component for (c) and (d).

#139089 - $15.00 USD Received 2 Dec 2010; revised 7 Jan 2011; accepted 10 Jan 2011; published 11 Jan 2011

In what follows, we discuss the lateral shifts as a function of the thickness of the slab under different angles of incidence. First, we consider the lateral shifts of the reflected wave from a negative chiral slab with the same parameters as in Fig. 3. We find that when θ_i is smaller than the pseudo-critical angle ($\theta_c \simeq 37^\circ$), the lateral shifts of the reflected perpendicular component could reach large positive or relatively small negative values, but there exists no periodic fluctuation of the lateral shifts with respect to the thickness as shown in Fig. 5(a). Similar phenomenon can be found from the shifts of the parallel component [see Fig. 5(c)]. The large positive enhancement corresponds to the dip of the reflection coefficients, which follows previous discussions. However, when θ_i is at the critical angle of the LCP wave, as shown in Figs. 5(b) and 5(d), the lateral shifts of both reflected components are always negative and the periodic fluctuation of the lateral shifts arises especially for the parallel component. Moreover, the fluctuations of the lateral shifts of both components first reach a maximally shifted distance, and then become saturated, keeping periodically fluctuating with respect to the thickness of the slab. In addition, if the angle of incidence θ_i is larger than the pseudo-critical angle and keeps increasing, the lateral shifts with periodic fluctuation under the same thickness of the slab will decrease, as shown in Figs. 5(b) and 5(d).

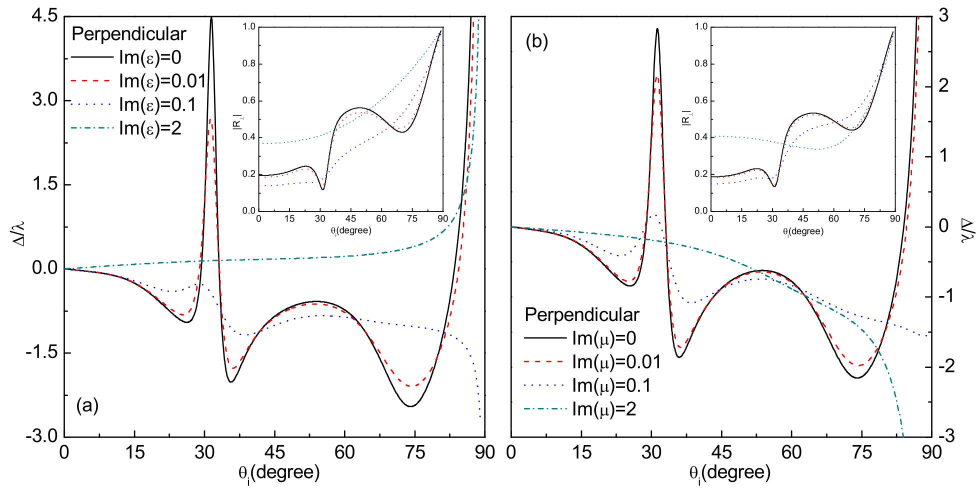

Fig. 6. The dependence of the lateral shift on the angle of incidence at different absorption scales. (a)$\mu = 1+0.02i$, (b)$\varepsilon = 0.64+0.02i$.

In order to demonstrate the role of the loss of the chiral slab, we further investigate the lateral shifts of the reflected perpendicular component at different absorption scales. Here we discuss two types of lossy chiral slabs, whose parameters are: (a) $\mu = 1+0.02i$, $\mathrm{Re}(\varepsilon) = 0.64$, (b) $\varepsilon = 0.64+0.02i$, $\mathrm{Re}(\mu) = 1$. The other parameters are the same: $\kappa = 1.4$, $d = 1.5\lambda$. The dependence of the lateral shifts on the angle of incidence is shown in Fig. 6. It can be seen that when the absorption of the chiral slab is weak, for the reflected perpendicular component, the behaviors of its lateral shift with respect to the angle of incidence for different dielectric loss or hysteresis loss are similar. However, the enhanced lateral shifts at the dip of the pseudo-Brewster angle will be always damped when the dielectric loss (see Fig.6(a)) or hysteresis loss (see Fig.6(b)) increases. On the other hand, when the absorption of the chiral slab becomes strong, the pseudo-Brewster angle disappears and the lateral shift becomes larger at close-to-grazing incidence. The insets of Fig. 6 show the reflected coefficients, from which we can also predict that the pseudo-Brewster angle (corresponding to the minimum of reflected coefficients) will disappear with increasing loss of the chiral slab. Here we notice that the high dielectric loss

#139089 - $15.00 USD Received 2 Dec 2010; revised 7 Jan 2011; accepted 10 Jan 2011; published 11 Jan 2011

and the high hysteresis loss will lead to the different behaviors of the lateral shifts with respect to the angle of incidence, i.e., the high dielectric loss results in the large positive lateral shift while the high hysteresis loss leads to the large negative lateral shift at close-to-grazing incidence. In addition, for reflected parallel component, the behavior of the lateral shifts in the presence of dielectric loss is analogous to that in the presence of hysteresis loss (not shown here).

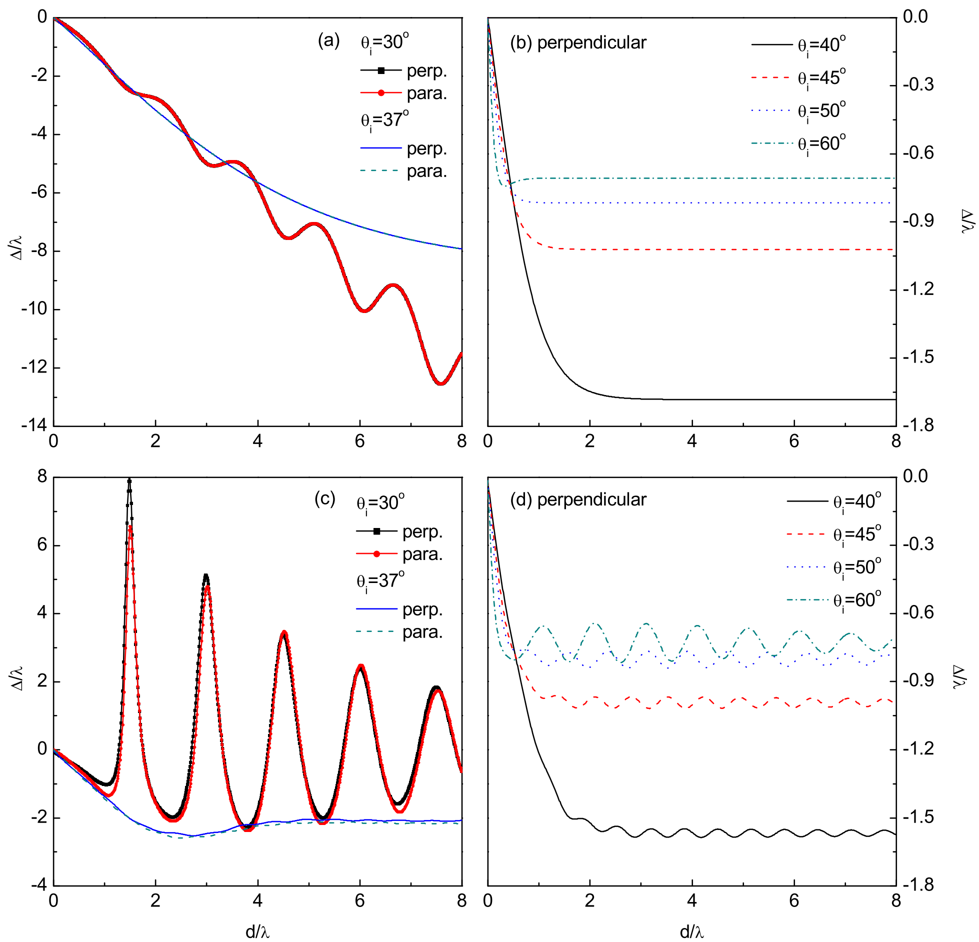

Fig. 7. The dependence of the lateral shift on the thickness of an invisible (for RCP wave) chiral slab at different θ_i.(a,b) lossless chiral slab; (c,d) lossy chiral slab.

Apart from the aforementioned negative chiral slab, we also consider the other lossless chiral metamaterial slab, as shown in Fig. 7. Here, we set the parameters of the chiral medium as $\varepsilon = 0.2$, $\mu = 0.2$, and $\kappa = 0.8$ in Fig. 7(a) and (b). In this situation, the wave number matching condition $k_1 = k_0$ and the wave impedance matching condition $\eta = \eta_0$ are satisfied simultaneously. Therefore the RCP wave is transmitted through the chiral medium without either reflection or refraction. Thus, the medium is invisible for RCP wave [35], whereas the LCP wave can be refracted and reflected, or totally reflected from the material. This unusual phenomenon can be physically understood as a destructive interference of electric and magnetic responses, due to the mixing through the chirality parameter. For $k_2 = -0.6k_0$, the critical angle for LCP wave is $\theta_c = \arcsin 0.6 \simeq 37^\circ$. Therefore, LCP wave is totally reflected with $\theta_i > 37^\circ$ and it is easy to see that both reflected components have the same negative lateral shift. This is due to the fact

#139089 - $15.00 USD Received 2 Dec 2010; revised 7 Jan 2011; accepted 10 Jan 2011; published 11 Jan 2011

that the reflected wave only has LCP wave, and the RCP wave contributes to the transmitted wave. Hence the perpendicular and the parallel reflection coefficients have the same absolute values, while their phases are different. We further find the lateral shifts will fluctuate with respect to the thickness of the slab when the angle of incidence is smaller than the critical angle of the LCP wave ($\theta_i < \theta_c$), while for $\theta_i \geq \theta_c$, the lateral shifts will vary with the thickness monotonously. We believe that the difference of the behavior of the lateral shifts is caused by the change of the properties of the LCP wave, i.e, the LCP wave changes from the transmitted wave to an evanescent wave. Meanwhile, when the angle of incidence is close to the critical angle of the LCP wave, the lateral shifts are large and increase as the slab thickness increases. If the angle of incidence is greater than θ_c, the lateral shifts will increase quickly and then gradually approach to an asymptotic negative value with increasing the slab thickness(see Fig. 7(b)). In this connection, the phenomenon that the lateral shifts become saturated as the thickness increases is due to the Hartman effect.

Furthermore, in order to show the influence of the absorption of the chiral slab on the lateral shifts, we plot the dependence of the lateral shift on the thickness of a lossy chiral slab for $\varepsilon = 0.2 + 0.01i$, $\mu = 0.2 + 0.02i$, and $\kappa = 0.8$, as shown in Fig. 7(c) and 7(d). The results show that: (1) both reflected components almost have the same lateral shifts; (2) the lateral shifts of both reflected components will fluctuate strongly with respect to the thickness of the slab for $\theta_i < \theta_c$. Moreover, for $\theta_i > \theta_c$, the larger the angle of incidence is, the stronger the periodic fluctuation becomes along the lossy chiral slab.

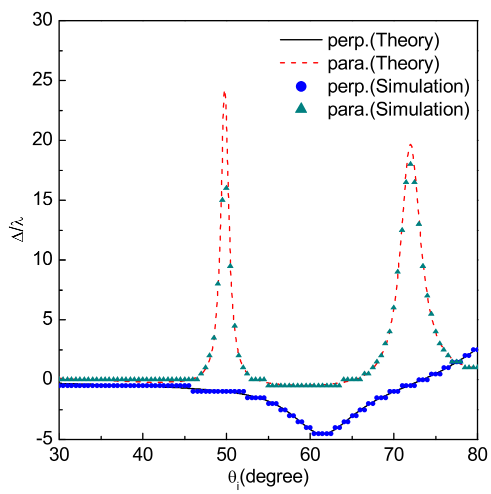

Fig. 8. Dependence of the lateral shift on the incident angle. The theoretical result is shown by the line; the numerical results (for $w_0 = 20\lambda$) are shown by scatters, all the other optical parameters are the same as in Fig. 3(a).

In the end, to show the validity of the stationary-phase method, we further perform numerical simulations with a two-dimensional incident Gaussian-shaped light beam. The electric fields ($E^r_\perp$ and $E^r_\parallel$) of the reflected beam are directly determined from Eq. (23). The calculated beam shift can be obtained by finding the location where $\left|E^r_\perp\right|_{z=0}$ or $\left|E^r_\parallel\right|_{z=0}$ is maximal [10]. Figure 8 shows the simulated data of curves in Fig. 4(a). For comparison, both the numerical and theoretical results are shown in Fig. 8. At $w_0 = 20\lambda$, the peaks of the numerical shifts are: -4.5λ for the perpendicular reflected field; and 16.5λ (dip I), and 18λ (dip II) for the parallel reflected field. The peaks of the theoretical shifts are about -4.54λ for the perpendicular field

#139089 - $15.00 USD Received 2 Dec 2010; revised 7 Jan 2011; accepted 10 Jan 2011; published 11 Jan 2011

and 24.25λ (19.66λ) for dip I (dip II) of the parallel field. It is noted that the discrepancy between theoretical and numerical results is due to the distortion of the reflected beam, especially when the waist of the incident beam is narrow [36]. Further numerical simulation shows that the wider the incident beam is, the smaller the discrepancy is.

4. Conclusion

In summary, an investigation on the lateral shifts of both reflected parallel and perpendicular components for the lossy chiral metamaterial slab has been done by using the stationary-phase approach. We show that the lateral shifts of the reflected perpendicular components can be large negative as well as positive near pseudo-Brewster angle, at which $|R|$ reaches a minimum. In addition, at a given incident angle, the dependence of the lateral shifts on the slab thickness for a negative chiral slab has also been studied. It is shown that, when the angle of incidence is at the critical angle of the LCP wave, the lateral shifts of both reflected components oscillate. Along with the increasing thickness of the slab, the shifted distance is increasing first, experiences a maximum value, and then arrive at the saturation (i.e., the periodic fluctuation of the lateral shifts when the slab's thickness is sufficiently big). Moreover, when the angle of incidence is larger than the critical angle and keeps increasing, the lateral shifts of both reflected components will decrease along with slab's thickness. In addition, we calculate the lateral shifts of an invisible chiral medium with and without loss. In order to demonstrate the validity of the stationary-phase approach, numerical simulations are made for a Gaussian-shaped beam.

Some other comments are in the following. Though the lossless parameters of the chiral material have been discussed in references [12, 13, 37–39], the realistic chiral material is dissipative. Here we take the absorption into account by adding imaginary parts to the parameters (such as ε and μ). Alternatively, one can also adopt the Drude model for ε and μ, and the Condon model for the chirality κ [40], in order to consider the effect of the dispersion within our method. As for the observability of the lateral shift in our paper, the magnitude of the reflectivity from the chiral slab is about $0.001 \sim 0.02$, which is larger than that (10^{-3}) of the semiconductor [41]. Therefore, the lateral shift of the reflected beam near the Brewster angle is also detectable as discussed in Ref. [41]. In this regard, the shift may be determined by finding the spot of the maximum intensity with detectors, since the reflection (although it is weak) is still Gaussian as long as the incident beam is Gaussian with a large beam width. In our case, since the 2D TE incident wave is considered, one only needs to investigate the lateral shift, i.e., we confine ourselves to a 2D problem to focus on the lateral shift. However, for a 3D incident wave on an isotropic material, both lateral and transversal (Imbert-Fedorov) shifts may appear simultaneously [42–44]. It would be of great interest to study the Imbert-Fedorov shifts from the chiral metamaterial slab.

Acknowledgments

This work was supported by the Key Project in Science and Technology Innovation Cultivation Program and the plan of Dongwu Scholar, Soochow University.